Relative single- and double-photoionization cross sections of Mg around the $2p \rightarrow nl$ resonances

R. Wehlitz* and P. N. Juranić†
Synchrotron Radiation Center, University of Wisconsin-Madison, Stoughton, Wisconsin 53589, USA
(Received 4 November 2008; published 13 January 2009)

Using highly monochromatized synchrotron light and the ion time-of-flight method to detect singly and doubly charged magnesium ions, we have measured relative single- and double-photoionization cross sections of Mg from 55 to 58 eV, which includes the region of the $2p \rightarrow nl$ inner-shell excitations. The resonances were analyzed using Fano profiles and the resonance positions are compared to previously published data. The quantum defect theory is applied to the resonance energies revealing that the published Mg $2p_{1/2}$ and $2p_{3/2}$ thresholds need to be revised. In addition, we have determined the double-to-single photoionization ratio in the 55 to 71 eV region.

DOI: 10.1103/PhysRevA.79.013410 PACS number(s): 32.80.Fb

I. INTRODUCTION

Recently we have measured the double-to-single photoionization ratio of magnesium below 55 eV, before the $2p \rightarrow nl$ resonances start to contribute to the double photoionization cross section via autoionization, a process in which two electrons are emitted sequentially. Photoabsorption spectra of Mg have been recorded in the past [1–3] but suffered from a low energy resolution or may have contained artificial peaks due to the vuv light created by sparks [1,2]. Although the experiment conducted by Ederer *et al.* [3] used synchrotron light to investigate the Mg $2p$ inner-shell excitations, this experiment as well as the other two experiments relied on the accurate measurement of the plate density and a high quality photofilm. Excitation by electron impact is not considered here because the dipole selection rules that are valid for photoexcitation do not apply to particle impact and complicate an analysis of the resonances.

Thus, our goal is to provide experimental data with a high energy resolution not only for the total but also for the single- and double-photoionization cross section in the $2p \rightarrow nl$ resonance region. Moreover, we are interested in extending the double-to-single photoionization ratio to higher photon energies than was done in a previous experiment [4]. The work described in this paper was done to provide state-of-the-art experimental data for testing advanced theories when they become available. Magnesium—although a small closed-shell atom—is a challenging target as it already needs to be treated relativistically in theoretical models. Moreover, our work provides high-resolution data for calibration purposes in the 50 eV photon energy range, which may become useful in light of continuing improvements of beamlines and monochromators.

II. EXPERIMENT

A. Experimental setup

The experiment was performed on the plane-grating-monochromator undulator (U3) [5] beamline at the Synchrotron Radiation Center in Stoughton, Wisconsin. The PGM beamline was employed for measurements in the 55 to 71 eV photon energy range, where the $2p \rightarrow nl$ resonances of Mg occur. The undulator was scanned simultaneously with the monochromator in steps of 2 meV while recording either the Mg^+ or Mg^{2+} ions. Above 58 eV, we took individual ion time-of-flight spectra in steps of 0.5 eV. Using a 17 μm entrance and 10 μm exit slit we achieved an energy resolution of 5.3 meV in the 55–58 eV energy region. Second-order light, which affects the photoionization cross sections, was sufficiently suppressed with a 0.5 μm aluminum filter. The photon flux was monitored with an xuv-100 photodiode and recorded together with the ion data during the photon energy scans.

As in our previous experiments, the monochromatized photon beam passed through a differential pumping stage which held our filter arrays. A capillary connected the differential pumping stage and the main chamber and was aligned so that the photon beam went through it with a minimal photocurrent on the capillary (typically less than 100 pA).

The photon beam entered the interaction region in the main chamber, where it photoionized the Mg atoms produced by a resistively heated oven. The Mg was heated to a temperature of about 390 °C. The Mg used in the experiment had a 99.5% metal purity. Before loading it into the oven the surface was scraped clean with a knife.

The ion time-of-flight (TOF) spectrometer used to detect the Mg ions consists of a pusher plate, extractor plate, drift tube, and a Z stack of microchannel plates (MCP) [6]. A pulsed electric field of 25 V/cm was applied to the pusher plate, which accelerated the photoions towards the grounded extractor plate equipped with a high-transmission copper mesh. The ions got further accelerated towards the drift tube by a permanent 250 V/cm electric field. After flying through the 15.4 cm long drift tube, which is terminated on either side by a copper mesh, the ions were accelerated onto a commercial (Hamamatsu) MCP detector. Each pulse created by the MCP detector was discriminated against noise by a constant-fraction discriminator set at its lowest threshold of 28 mV. This pulse was the start signal for the TOF measurement and the following electric pulse applied to the pusher plate provided the stop signal. The flight-time measurement was performed by a time-to-amplitude converter that provided the input for a computer interface and its multichannel-

*wehlitz@src.wisc.edu
†Present address: HASYLAB at DESY, Notkestrasse 85, 22607 Hamburg, Germany.

analyzer software. A sketch of the experimental setup and information on the experimental parameters that are important for ion TOF measurements can be found in Ref. [7]. The count rate was low enough so that dead time problems did not occur.

B. Data analysis

We extracted the areas of the singly and doubly charged ion peaks in our time-of-flight spectra using direct numerical integration. The ion scans were normalized with the photon flux and background corrected. Neon was used to calibrate the beamline's photon energy by measuring the ion signal while scanning the monochromator across the Ne $2s \rightarrow 4p$ and $5p$ resonances at 47.1193(50) eV and 47.6952(15) eV, respectively [8]. Our data were energy corrected with the average wavelength offset calculated from these two resonances.

For a quantitative analysis of the $2p \rightarrow nl$ resonances we have applied the Fano formula [9] with an additional slowly varying background σ_b to our data

$$\sigma = \sigma_a \frac{(q+\epsilon)^2}{1+\epsilon^2} + \sigma_b, \tag{1}$$

where $\epsilon = 2(E - E_0)/\Gamma$. Here, q is Fano's profile parameter, E is the photon energy, E_0 is the energy position of the resonance, and Γ is the resonance width. σ_a represents the part of the continuum cross section that interacts with the discrete level. In order to fit the Fano profiles to the resonances, Eq. (1) was convoluted with a Gaussian bandpass. At first the bandpass was a free parameter in our Fano fits of the Mg^+ and Mg^{2+} ion yields and remained stable within 0.5 meV. In order to determine the widths of the resonances we applied a fixed average value of 5.3 meV to all fits.

The resonances appear in groups forming five Rydberg series that converge to series limits that mark the two $2p$ inner-shell thresholds. The Rydberg series have been analyzed using the quantum defect theory, i.e., the resonance positions E_0 as a function of the principal quantum number n have been fitted according to

$$E_0(n) = E_\infty - R/(n-\delta)^2. \tag{2}$$

Here, E_∞ is the series limit, R is the Rydberg constant (13.6058 eV), and δ is the quantum defect. This equation works well for high principal quantum numbers n but is less accurate for low n because the excited electron is closer to the nucleus and thus more perturbed by its neighboring electrons.

III. RESULTS AND DISCUSSION

A. Total cross section

Before we go into more details, we want to present our total photoionization cross-section data obtained by adding the measured relative single- and double-photoionization cross sections. The resulting curve (black line) is shown along with the digitized photoabsorption spectrum of Ederer *et al.* [3] in the upper panel of Fig. 1 which is depicted as a dotted line. While the agreement appears to be poor, shifting and compressing the absorption spectrum yields a fairly good agreement as can be seen by the resulting gray line. Obviously, our energy resolution is much better yielding narrower resonances in the spectrum. Note that the change of the energy scale was only necessary for the spectrum digitized from their paper [3]. As we will see later, the energy positions that they give in their tables do not require any energy correction. Above 57 eV their absorption spectrum shows a rising background possibly due to the $2p$ thresholds and their rather large photon energy bandpass. A total cross-section spectrum in the 54–59 eV photon energy range has been also derived by Whitfield *et al.* [11] by adding the partial cross section channels of the $3s$ main line and various correlation satellites. Since this experiment was performed with a much lower energy resolution we did not include it in Fig. 1.

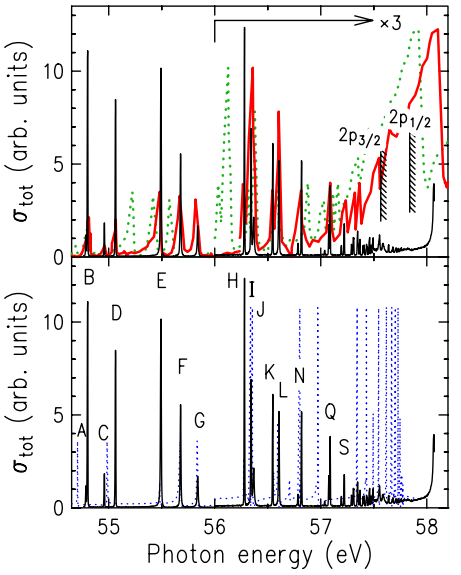

FIG. 1. (Color online) Total photoionization cross section of Mg in the $2p \rightarrow nl$ resonance region (solid black line). The upper panel also shows the total cross section curve of Ederer *et al.* [3] (dotted line). The same curve has been shifted and compressed (gray line) for a better agreement with our data. The lower panel shows the calculated cross section for the $3s^2 \rightarrow 3skp(^1P)$ transitions in the $2p \rightarrow nd, ns$ resonance region [10] (dotted line) along with our data. The peaks in the theoretical data are cut off as they appear in the original presentation. The resonances are labeled by letters for identification purposes. Note that in both panels all data are multiplied by 3 above 56 eV.

A theoretical calculation by Altun [10] using many-body perturbation theory is shown as a dotted line in the lower panel of Fig. 1. This curve was digitized from a figure where most lines were cut off at the top so that a meaningful scaling of the theoretical to the experimental resonances was not attempted. There is a reasonably good agreement of the resonance positions in the 55.4 to 56.8 eV region. However, the theoretical positions of the two lowest resonances ($2p^5 4s$) are too low and the resonances above 56.8 eV do not have an easy-to-find counterpart in the experimental spectrum. The latter problem may be due to the resonances being extremely narrow, too narrow to show up in the experimental spectrum

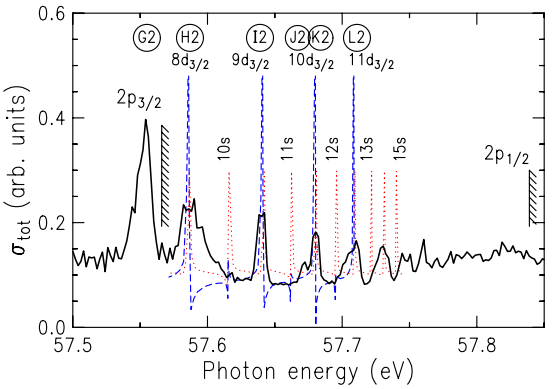

FIG. 2. (Color online) Our total photoionization cross section of Mg between the $2p_{3/2}$ and $2p_{1/2}$ thresholds (solid black line) along with the theoretical $3s$ (dashed line) and $2p_{3/2}$ (dotted line) cross sections of Deshmukh and Manson [12]. Note that the tips of all calculated resonances are cut off. The theoretical curves are shifted by about 4.4 eV to lower energies. The resonances are labeled by letters inside circles for identification purposes.

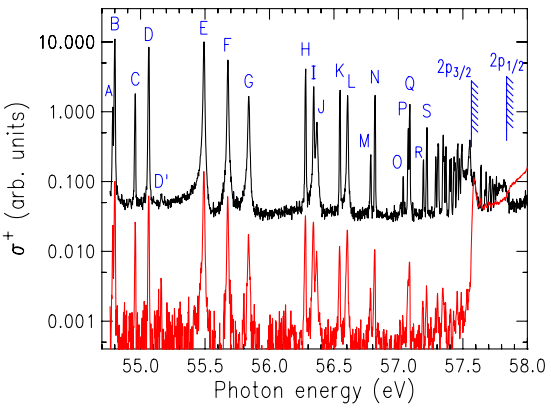

FIG. 3. (Color online) Relative single (black) and double (gray) photoionization cross sections of Mg. Note that the cross sections are displayed on a log scale. The resonances are labeled by letters and the $2p$ thresholds are indicated in the figure.

or due to an overestimate of the strength of those resonances.

In a theoretical study, Deshmukh and Manson [12] have employed the relativistic random-phase approximation in order to calculate the Mg $3s$ and $2p_{3/2}$ cross sections between the $2p_{3/2}$ and $2p_{1/2}$ thresholds. We show their results in Fig. 2 along with our total cross section. In order to achieve a satisfactory agreement, we have shifted the energy scale of the theoretical data by about 4.4 eV and stretched them by about 10% such that the first resonance, $2p \rightarrow 8d_{3/2}$, lines up with the experimental resonance and the theoretical $2p_{1/2}$ threshold is at the experimentally determined position. The energies used in the calculation are Dirac-Fock energies that are not expected to be very accurate [13]. With this treatment we obtain indeed a good agreement with all theoretical resonance positions although the *ns* resonances are hardly visible in our spectrum. The assignments for some of the resonances in Fig. 2 differ from the ones in the original paper [12] due to a mislabeling in their figure [13].

B. Single- and double-ionization cross sections

Figure 3 shows the single- and double-photoionization cross sections in the $2p \rightarrow nl$ resonance regions on a relative scale. However, the spectra are properly normalized with respect to each other. We used a logarithmic scale for the cross sections to make smaller features more visible. In order to identify the resonances we have labeled them with letters. Most resonances look essentially symmetric and only a few reveal some asymmetry when fitted to a Fano profile. The region around the $2p$ thresholds is shown in Fig. 4. Some of the higher resonances such as "H2" and "I2" are most likely more than one resonance although we have fitted them as one resonance since they were not sufficiently resolved.

The thresholds for the $2p_{3/2}$ and $2p_{1/2}$ electrons are marked with a comb and were derived by applying the quantum defect theory to the different Rydberg series converging to those thresholds. As we will see later, these thresholds are different from the ones in the literature, which are indicated as dotted lines in Fig. 4. The new, revised thresholds are at the expected positions. At the $2p_{3/2}$ threshold, the double-photoionization cross section rises steeply due to the dominant inner-shell ionization leading to a nonresonant Auger decay which results in a doubly charged Mg ion. At the second inner-shell threshold ($2p_{1/2}$) the slope in the double- and single-ionization cross sections changes, i.e., the double-ionization cross section rises further while the single-ionization cross section decreases slightly. These changes in the cross sections are not as obvious for the older values for the thresholds. Note that the steep increase in the number of Mg^{2+} ions starts slightly below the $2p_{3/2}$ threshold because of the finite monochromator bandpass of 5.3 meV.

As mentioned above, we have fitted the resonances using a Fano profile, given in Eq. (1), convoluted with the monochromator bandpass. The results are presented in Table I along with the energy positions presented by Newsom [1], Ederer *et al.* [3], and NIST [14]. We note that Eq. (1) is valid only for an isolated resonance interacting with one continuum. Although the resonances are rather closely spaced in energy, their distance from each other is typically much larger than their widths, i.e., in critical cases the resonance

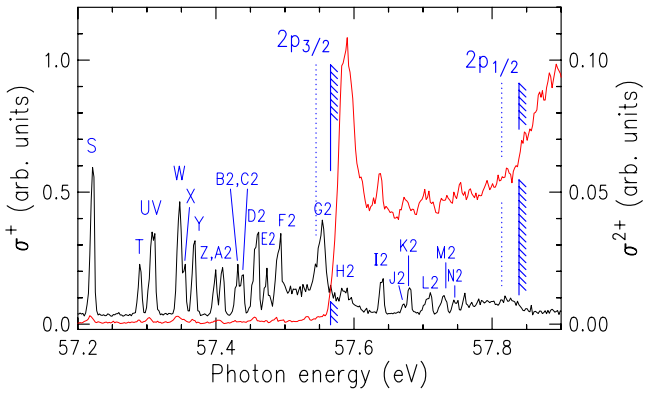

FIG. 4. (Color online) Relative single (black) and double (gray) photoionization cross sections of Mg near the $2p$ thresholds. Besides the new, revised thresholds, the previously reported thresholds are indicated as dotted lines.

TABLE I. Experimental resonance positions E_0, widths Γ, and Fano-parameters q of the Mg $2p \rightarrow nl$ resonances in the single- and double-photoionization cross section. The resonances are labeled as shown in our figures. The Rydberg series are numbered as follows: 1, $2p^5(^2P^o_{3/2})ns[3/2]$; 2, $2p^5(^2P^o_{1/2})ns[1/2]$; 3, $2p^5(^2P^o_{3/2})nd[3/2]$; 4, $2p^5(^2P^o_{3/2})nd[1/2]$; 5, $2p^5(^2P^o_{1/2})nd[3/2]$. Included are the resonance positions of Newsom [1], Ederer *et al.* [3], and the tabulated values of NIST [14].

		E_0 (eV)				Mg^+		Mg^{2+}
Resonance	Series	This work	Ref. [1]	Ref. [3]	Ref. [14]	Γ (meV)	q	q
A		54.785(2)				4.4(7)	∞	∞
B	1	54.801(1)	54.8006(17)	54.802(5)	54.8	1.3(1)	∞	∞
C		54.959(1)	54.9602(17)	54.962(5)	54.96	1.6(6)	∞	∞
D	2	55.064(1)	55.0645(17)	55.065(5)	55.065	2.1(7)	135.0(500)	∞
D′		55.162(3)						
E	3	55.492(1)	55.4916(15)	55.491(5)	55.492	4.6(9)	−47.0(200)	−40.0(150)
F	4	55.677(1)	55.6770(15)	55.678(5)	55.678	5.0(1)	∞	340.0(300)
G	5	55.838(1)	55.8377(15)	55.839(5)	55.839	8.2(4)	∞	103.0(300)
H	1	56.279(1)	56.2802(16)	56.277(5)	56.278	1.3(2)	−27.0(100)	−16.0(70)
I	3	56.342(1)	56.3421(13)	56.356(5)	56.342	3.4(3)	−27.0(100)	−16.0(70)
J	4	56.366(1)	56.3660(12)	56.356(5)	56.366?	11.0(9)	∞	∞
K	2	56.546(1)	56.5451(13)	56.544(5)	56.544	1.4(3)	∞	∞
L	5	56.605(2)	56.6032(13)	56.603(5)	56.604	4.5(4)	−21.0(100)	−13.0(60)
M	1	56.785(2)	56.7855(13)	56.777(5)	56.777	1.9(9)	−6.0(40)	
N	3,4	56.817(2)	56.8156(13)	56.816(5)	56.816	1.6(3)	−34.0(70)	
O	1,2	57.036(2)				<1.0		
P	3,4	57.075(2)	57.0809(16)	57.080(5)	57.080	1.7(9)	9.0(50)	
Q	5	57.088(2)			57.080	1.2(5)	−13.0(40)	
R	1	57.193(2)				<1.0		
S	3,4	57.220(2)	57.2179(16)	57.215(7)	57.216	1.3(9)	−17.0(70)	
T	1	57.289(1)				<1.0		
U	4	57.305(2)	57.3054(19)	57.299(7)	57.302	<1.0		
V	2,3	57.311(2)				<1.0		
W	5	57.347(2)	57.3465(19)	57.347(5)	57.346	2.5(5)	∞	
X	1	57.355(1)				<1.0		
Y	3,4	57.368(2)				1.4(9)	∞	
Z	1	57.400(1)				1.8(9)	−14.0(70)	
A2	3,4	57.407(3)				1.7(9)	∞	
B2	1	57.431(2)				~3	∞	
C2	3,4	57.438(2)				<1.0		
D2	1,3	57.459(3)	57.4557(21)			3.5(9)	−3.4(20)	
E2	2,3	57.474(2)				3.3(9)	∞	
F2	3,5	57.490(2)	57.4914(21)			~6	∞	
G2		57.555(1)	57.5474(18)	57.547(5)	57.547	11.0(9)	−6.6(8)	
H2	2,5	57.587(2)	57.5838(19)	57.589(5)	57.587	17.6(9)	∞	
I2	2,5	57.639(2)	57.6363(22)			2.4(6)	∞	
J2	5	57.673(2)				2.0(9)	−5.7(20)	
K2	2	57.679(1)				2.2(15)	−0.4(10)	
L2	2,5	57.711(2)				2.2(15)	∞	
M2	2,5	57.733(2)				3.0(18)	−1.8(10)	
N2	2,5	57.746(2)				>4	−2.6(20)	
O2	2,5	57.761(2)						
P2		58.067(2)	58.072(13)	58.067(5)	58.067			

distance is in the order of 10 meV with widths of ~2 meV. The worst case are the resonances "J2" and "K2" that are only 6 meV apart. A modified fit formula, that considers overlapping resonances, had no impact on resonance "K2" and only a small impact on resonance "J2," i.e., the resonance position shifted by 1 meV, which is still within the error bar. In most cases we find very good agreement with the previously presented energies, even with the ones of Ederer *et al.* although their digitized spectrum seemed to be on a skewed energy scale as can be seen in Fig. 1. In a few cases, such as the group of resonances "O," "P," and "Q," the measurements of Refs. [1,3] may not have resolved the three resonances and, therefore, give an averaged energy position of the resonances. We want to emphasize that even at the higher energies (including the "P2" resonance) the agreement of our energy positions with the older data is very good.

The measurements of Ederer *et al.* could not rule out that three of the resonances seen by Newsom at 57.4557, 57.4914, and 57.6363 eV are artifacts as these lines had not been observed in other experiments [2,3]. However, we can confirm their existence as resonances "D2," "F2," and "I2." We also note that the resonance observed by Ederer *et al.* at 56.356(5) eV consists in fact of two resonances ("I" and "J") as observed by Newsom.

In Table I we have included our assignment of the resonances to the five possible Rydberg series as used in the quantum defect fits described below. Some of the resonances seem to belong to two series, i.e., two resonances are overlapping so that they appear as one resonance in our spectrum. On the other hand, there are resonances that could not be assigned to any of the five Rydberg series—a problem that has already been pointed out by Newsom. These unassigned resonances may be double excitations involving a $2p$ and a $3s$ electron.

The widths of the resonances are very narrow and often narrower than 1 meV which is far below our energy resolution. Consequently, no reliable q parameter could be extracted from those narrow resonances. We note that the agreement of the resonance widths in the Mg^+ and Mg^{2+} channels is, as it should be, excellent for the resonances "A" to "L." The higher resonances are often too narrow and too weak in the Mg^{2+} channel to extract a reliable width. Therefore, we present only the widths determined from the Mg^+ ion yield. The higher resonances, in particular "H2" (cf. Fig. 2), may consist of more than one resonance so that the width is determined by the separation of the two unresolved resonances. The Fano q parameter that describes the asymmetry of a resonance is often infinity, meaning that the resonance is in fact symmetric.

Two Rydberg series converge to the $2p_{1/2}$ and three series to the $2p_{3/2}$ thresholds. Using the analysis of Newsom [1] as a guide, we started evaluating the two Rydberg series converging to the higher $2p_{1/2}$ threshold, because only these two series remain above the $2p_{3/2}$ threshold. So, we employed the quantum defect theory as given in Eq. (2) to these two Rydberg series and find that this equation is a good description for resonances with $n>5$. As can be seen in Fig. 5 we can identify resonances up to $n=14$ and the deviation from the ideal curve is only a few meV. However, the series limit is

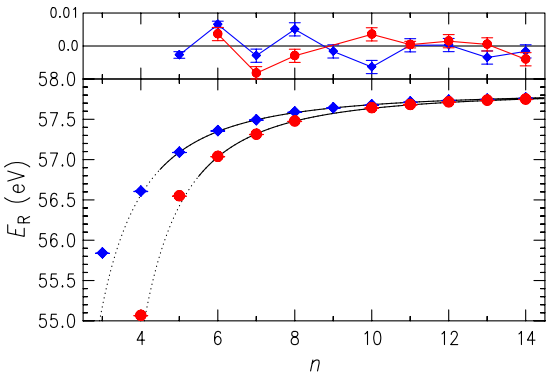

FIG. 5. (Color online) Resonance positions E_R as a function of the principal quantum number n for the two highest Rydberg series converging to the $2p_{1/2}$ threshold (circles, series "2," $2p^5(^2P_{1/2})ns[1/2]$; diamonds, series "5," $2p^5(^2P_{1/2})nd[3/2]$). The top panel shows the deviation of the data from the fit curve when applying Eq. (2) to our data. The fit was performed in the region of the solid line while the dotted line is an extrapolation of that fit.

about 27 meV higher than in previous measurements. We attribute this difference to the inclusion of higher n resonances not available before. This enables us to perform a more accurate extrapolation to the series limit. The fact that both series converge to the same (new) limit within their error bar gives us confidence that this is the correct value. Moreover, as mentioned above, our resonance positions agree with the older values so that this difference is not an artifact due to a faulty energy scale.

The same analysis was performed for the three lower Rydberg series using the data of Newsom [1] as a starting point. The corresponding quantum defect fits are shown in Fig. 6. As mentioned by Newsom the series "3" and "4" are blended for $n>4$ and are practically the same data for $n>4$ where the fit region begins. The fit for series "1" begins only for $n>6$. We achieve very good quantum-defect fits with deviations of only a few meV of our energies from the model

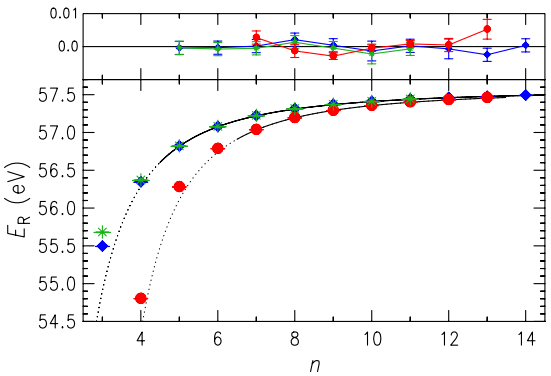

FIG. 6. (Color online) Resonance positions E_R as a function of the principal quantum number n for the three lower Rydberg series converging to the $2p_{3/2}$ threshold (circles, series "1," $2p^5(^2P_{3/2})ns[3/2]$; diamonds, series "3," $2p^5(^2P_{3/2})nd[3/2]$; asterisks, series "4," $2p^5(^2P_{3/2})nd[1/2]$). The top panel shows the deviation of the data from the fit curve when applying Eq. (2) to our data. The fit was performed in the region of the solid line while the dotted line is an extrapolation of that fit.

TABLE II. Five Rydberg series converging to the $2p_{3/2}$ and $2p_{1/2}$ thresholds with their quantum defect δ and series limit. Note that the quantum defects δ of Newsom [1] are the averaged values from individual members of a Rydberg series.

		δ		Limit (eV)		
Series	Assignment	This work	Ref. [1]	This work	Ref. [1]	Ref. [14]
1	$2p^5(^2P^o_{3/2})ns[3/2]$	1.94(2)	1.76	57.565(2)	57.5473	57.545
2	$2p^5(^2P^o_{1/2})ns[1/2]$	1.90(6)	1.87	57.843(2)	57.8250	57.814
3	$2p^5(^2P^o_{3/2})nd[3/2]$	0.74(1)	0.59	57.567(2)	57.5473	57.545
4	$2p^5(^2P^o_{3/2})nd[1/2]$	0.74(1)	0.55	57.568(2)	57.5473	57.545
5	$2p^5(^2P^o_{1/2})nd[3/2]$	0.74(1)	0.58	57.840(2)	57.8250	57.814

curves as can be seen in the upper panel of Fig. 6. All three series converge to the same series limit which, again, is higher than the previously presented value by about 21 meV.

Our results are summarized in Table II that shows the series limits as well as the quantum defects δ. The quantum defects for the series "1" and "2," which have an excited s electron, have a very similar δ of $\sim$1.9 that is in qualitative agreement with the average δ values by Newsom. We should note here that Newsom did not derive an average δ as we do, but calculates a δ for each member of the Rydberg series. Therefore, we have averaged his δ values for comparison. The series "3" to "5," which have an excited d electron, have the same quantum defect of 0.74 that is in qualitative agreement with the numbers of Newsom. As mentioned before, our series limits are higher but consistent. We tested their "stability" by performing quantum-defect fits [employing Eq. (2)] over different ranges of n. Naturally, a fit range for higher n should give a better result because quantum defect theory is a better approximation. However, one needs to include a sufficient number of resonance positions to achieve a small error bar. From the various tests we conclude that the Mg $2p_{3/2}$ threshold is at 57.566(2) eV and the Mg $2p_{1/2}$ threshold is at 57.841(2) eV.

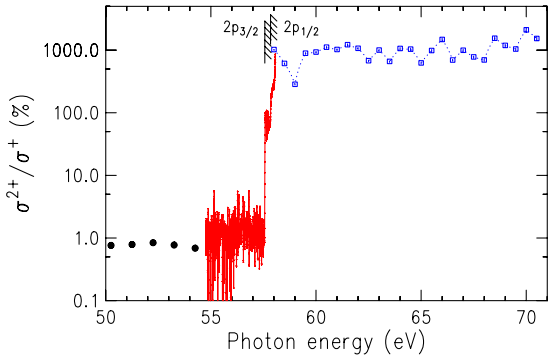

FIG. 7. (Color online) Double-to-single photoionization ratio of Mg on a logarithmic scale. The data depicted by a gray line were calculated from the photon energy scans for Mg^+ and Mg^{2+} across the resonances. The squares (connected by a dotted line) are the ratios calculated from individual ion TOF spectra. The black circles are previously presented [4] nonresonant ratios. The $2p$ thresholds are indicated in the figure.

C. Double-to-single ionization ratio

From the single- and double-photoionization cross sections in the 55–58 eV photon energy region we have calculated the corresponding double-to-single ionization ratio. In addition, we have taken ion TOF spectra in the 58–71 eV energy region from which we determined the ratios for higher energies. In Fig. 7 we show all Mg ratios in the 50–71 eV energy region on a logarithmic scale. The ratio above the $2p$ thresholds exhibit some scatter that may be due to other resonances, but stays approximately flat at 1000%, i.e., the double-photoionization cross section is about 10 times larger than the single-photoionization cross section. While these data still have a high photon energy resolution, our step size of 0.5 eV is much too large to identify individual resonances.

Figure 8 shows the double-to-single photoionization ratio in the $2p \rightarrow nl$ resonance region. Interestingly, not all resonances show up in the ratio but only the resonances "H," "I," "K," "L," and "N" are clearly visible. Due to the very low nonresonant intensity in the Mg^{2+} signal the ratio is somewhat noisy. Nevertheless, another resonance marked with "?" is showing up. A closer inspection of the single- and double-photoionization scans reveals that there is indeed a very small resonance that we have labeled "D′" in Table I. It is not clear to us why only these particular resonances appear so pronounced in the ratio while others are buried in the noise.

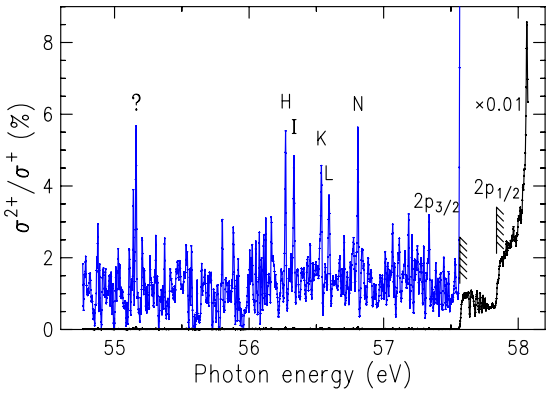

FIG. 8. (Color online) Double-to-single photoionization ratio of Mg in the $2p \rightarrow nl$ resonance region. The ratios above the $2p_{3/2}$ threshold are divided by 100.

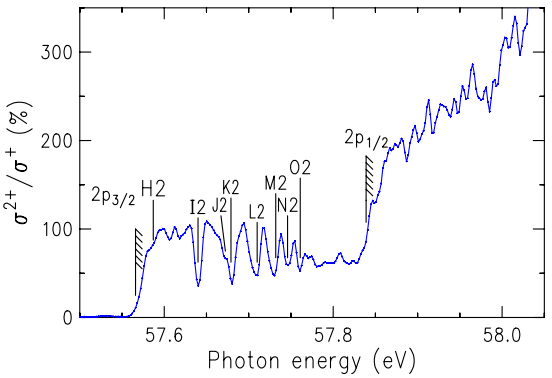

FIG. 9. (Color online) Double-to-single photoionization ratio of Mg near the $2p$ thresholds. The data have been smoothed for clarity.

Above the $2p_{3/2}$ threshold the ratio jumps up and jumps up again above the $2p_{1/2}$ threshold, which is shown in Fig. 9 on an expanded energy scale. In the figure we have indicated some of the resonance positions indicating that the resonances actually reduce the ratio as they appear as dips. From this figure one can suspect that resonance "H2" may consist of three resonances (see also Fig. 2).

IV. SUMMARY

We have measured the double-to-single photoionization ratio in the 55–71 eV region and the relative single- and double-photoionization cross sections between 55 and 58 eV with high photon energy resolution. Employing the Fano formula, Eq. (1), we have determined the energy positions, widths, and Fano q parameters of the $2p \rightarrow nl$ inner-shell resonances. Our resonance energies compare favorably with the resonance positions previously measured by Newsom [1] and Ederer *et al.* [3] and with the values listed by NIST [14]. However, we find that both presented Mg $2p$ thresholds are in fact more than 20 meV higher by employing the quantum defect theory to the corresponding Rydberg series. We obtain threshold energies of 57.566(2) eV and 57.841(2) for the $2p_{3/2}$ and $2p_{1/2}$ inner shells, respectively.

We have presented the double-to-single photoionization ratio that shows some of the resonance structure due to the $2p$ excitations. Above the $2p_{3/2}$ threshold, these resonances show up as dips in the ratio resulting in a decreased ratio on resonance. Overall, the ratio increases stepwise at both $2p$ threshold so that the double ionization cross section becomes more than 10 times larger than the single ionization cross section.

ACKNOWLEDGMENTS

The authors wish to thank the staff of the Synchrotron Radiation Center for their excellent support. We also thank Dr. S. Whitfield for a critical reading of the paper. This work is based upon research conducted at the Synchrotron Radiation Center, University of Wisconsin-Madison, which is supported by the NSF under Grant No. DMR-0537588.

[1] G. H. Newsom, Astrophys. J. **166**, 243 (1971).
[2] J. M. Esteva and G. Mehlman, Astrophys. J. **193**, 747 (1974).
[3] D. L. Ederer, T. B. Lucatorto, and G. Mehlman, J. Opt. Soc. Am. **69**, 520 (1979).
[4] R. Wehlitz, P. N. Juranić, and D. V. Lukić, Phys. Rev. A **78**, 033428 (2008).
[5] R. Reininger, S. L. Crossley, M. A. Lagergren, M. C. Severson, and R. W. C. Hansen, Nucl. Instrum. Methods Phys. Res. A **347**, 304 (1994).
[6] R. Wehlitz, D. Lukić, C. Koncz, and I. A. Sellin, Rev. Sci. Instrum. **73**, 1671 (2002).
[7] R. Wehlitz, M. M. Martinez, J. B. Bluett, D. Lukić, and S. B. Whitfield, Phys. Rev. A **69**, 062709 (2004).
[8] K. Schulz, M. Domke, R. Püttner, A. Gutiérrez, G. Kaindl, G. Miecznik, and C. H. Greene, Phys. Rev. A **54**, 3095 (1996).
[9] U. Fano, Phys. Rev. **124**, 1866 (1961).
[10] Z. Altun, Phys. Rev. A **40**, 4968 (1989).
[11] S. B. Whitfield, C. D. Caldwell, and M. O. Krause, Phys. Rev. A **43**, 2338 (1991).
[12] P. C. Deshmukh and S. T. Manson, Phys. Rev. A **28**, 209 (1983).
[13] S. T. Manson (private communication).
[14] Yu. Ralchenko, A. E. Kramida, J. Reader, and NIST ASD Team, NIST Atomic Spectra Database (version 3.1.5), http://physics.nist.gov/asd3 (National Institute of Standards and Technology, Gaithersburg, MD, 2008).